Heterogeneity of Subsurface Pore Distribution: Characterization based on Pressure and Tracer Responses to Identify Undiscovered Permeable Structures in Reservoirs

Mitsuo Matsumoto[1] and Kazuki Sawayama[2]

[1]Department of Earth Resources Engineering, Faculty of Engineering, Kyushu University, Japan.

[2]Institute for Geothermal Sciences, Kyoto University, Japan.

Corresponding author: Mitsuo Matsumoto (matsumoto@mine.kyushu-u.ac.jp)

Key Points:

- This study proposed and validated a concept for quantifying the heterogeneity of subsurface pore distribution.
- The concept combines conventional pressure transient and tracer testing, assuming diffusion and advection–dispersion problems.
- This concept provides a useful scale to quantify undiscovered permeable structures in exploring and developing reservoirs.

Abstract

Pressure transient and tracer testing are conventional methods employed to investigate physical properties associated with fluid flow and/or storage in subsurface reservoirs or aquifers. These methods have been adopted independently to investigate from different physical aspects. Here, to quantify the heterogeneity of pore distributions containing subsurface fluid, a novel concept, which combines the pressure and tracer concentration responses obtained during pressure transient and tracer tests, respectively, has been proposed and validated. Herein, the key parameter is the difference between the apertures of the equivalent planar fractures estimated from the pressure and tracer concentration responses. In particular, this difference is attributed to the fact that the pressure and tracer concentration responses obey different physical mechanisms, diffusion and advection–dispersion problems, respectively, that generate dissimilar responses to the heterogeneity of pore distribution. The concept was successfully validated using laboratory experiments and reservoir simulations conducted at multiple scales. As observed, the apparent pore volume estimated from the pressure responses tended to be larger than the actual value owing to the delay in pressure responses during propagation through the pore. By quantifying the existence of undiscovered permeable structures in a reservoir simulation model, the proposed concept provides an insightful guide for successful decision-making in explorational and developmental geothermal projects. Furthermore, the concept provides a scale for assessing the accuracy of a reservoir simulation model in expressing an actual heterogeneous permeable structure.

Plain Language Summary

Conventionally, the physical properties of subsurface structures such as reservoirs or aquifers involving flow and/or storage of fluids (e.g., water, oil, and gas) are investigated using two testing methods: pressure transient test and tracer test. The pressure transient test measures the pressure variations occurring during production and/or injection of fluid using wells, whereas the tracer test monitors the variations in the concentration of tracers (e.g., ionized substances and stable isotopes) at production wells and springs. This study combined the pressure and tracer testing methods to propose a novel concept and validated it to quantify the complexity of the pore distribution of a reservoir or aquifer containing branches and dead ends. This concept utilizes the difference in physical mechanisms that pressure and tracer concentration obey,

diffusion and advection–dispersion problems, respectively. The concept was successfully validated using laboratory experiments and computer simulations. Overall, the concept can provide an insightful guide for successful decision-making in explorational and developmental geothermal projects by quantifying the existence of undiscovered permeable structures in reservoir simulation models. Furthermore, the proposed concept provides a scale for reservoir simulation models to accurately express an actual complex reservoir or aquifer.

Keywords

heterogeneity, pressure transient testing, tracer testing, reservoir modeling, exploration and development, geothermal project

1 Introduction

Adequate understanding of subsurface fluid flow under heterogeneous pore distribution is key to successfully resolve numerous geoscientific and engineering problems. As such, heterogeneity is generated in a wide range of scales, including an outcrop of several tens to hundreds of meters associated with a fracture network (Bisdom et al., 2016; Zuo et al., 2019) and a fault intersecting a field spanning several kilometers (Erdogmus et al., 2006; Goko, 2000; Rae et al., 2004). A reliable and direct approach for investigating fluid flow under such conditions involves the observation of in situ responses such as temporal variations in pressure and solute concentration at one or more observational points, while generating artificial flow at a scale corresponding to the given problems. Pressure transient and tracer testing methods are popular conventional methods that can estimate the physical parameters, productivity, performance, and mass transfer associated with fluid flow and/or storage in subsurface reservoirs or aquifers at a field scale.

Pressure transient testing measures the pressure responses during production and/or injection of fluid to estimate several parameters such as transmissivity, storativity, skin factor, and wellbore storage constant by modeling fluid flow in a reservoir surrounding the wellbore according to Darcy's law (Agarwal et al., 1970; Bourdet et al., 1983; Theis, 1935; van Everdingen & Hurst, 1949; van Everdingen, 1953). In the oil and gas industry, several key parameters such as reservoir size, geometry, total pore volume, and mechanisms supporting reservoir pressure are estimated for project feasibility studies, considering essential information

on recoverable reserves and forecasted decline in production (Horne, 1995; Houzé et al., 2012). Historically, the geothermal industry has applied several techniques developed in the oil and gas industry. In the geothermal industry, pressure transient testing employs a reservoir simulation model to estimate the possible production and reinjection rates for continuous sustainable power generation across several decades (DiPippo, 2016; Grant & Bixley, 2011; Zarrouk & McLean, 2019). Assuming that type curves obey several extended models to express heterogeneity, such as the leaky aquifer (Hantush, 1956), dual-porosity model (Barenblatt et al., 1960; Warren & Root, 1963), linear and bilinear flows associated with a fracture (Cinco-Ley et al., 1978; Gringarten et al., 1974), MINC model (Pruess & Narasimhan, 1982, 1985), fractional dimension models (Acuna & Yortsos, 1995; Chang & Yortsos, 1990), and other flexible numerical models using application software such as AWTAS (O'Sullivan et al., 2005) and Saphir (Houzé et al., 2012), reservoir engineers have been able to interpret and estimate the pressure responses under diverse conditions. The models commonly used for analyzing pressure responses obey the diffusion problems for both quasi-incompressible and compressible fluids by adopting pseudo-pressure (Al-Hussainy et al., 1966).

Tracer testing uses flowing wells to inject a tracer into an injection well and measure the tracer concentration responses at the production wells. Referring to the tracer concentration responses and obeying advection–dispersion problems, the direction and velocity of subsurface fluid flow along with multiple properties such as porosity, dispersibility, hydrostratigraphy, and heat transfer characterization have been successfully determined (Grove & Beeten, 1971; Güven et al., 1986; Hall, 1993; Klepikova et al., 2016; Leaf et al., 2012; Mackay et al., 1986; Reimus et al., 2003). For several decades, a variety of tracers have been adopted, e.g., solid particles, ionized substances, stable isotopes, radioactive substances, organic dyes, gases, and fluorocarbons, as well as water temperature (Davis et al., 1980). In principle, tracers must satisfy several conditions such as detectivity, chemical stability, negligible absorption, and absence in a natural state. Additionally, reactive tracers have been adopted for advanced techniques (Adams & Davis, 1991; Davis et al., 2000; Lemke et al., 2013). Comprehensively, tracer testing is applied across a diverse range of subsurface fluid fields such as the oil and gas (Cockin et al., 2000; Patidar et al., 2022; Tomich et al., 1973) and geothermal (Chrysikopoulos, 1993; Rose et al., 2001; Sanjuan et al., 2006) industries. In tracer testing, investigating and characterizing the heterogeneity of the above-mentioned physical properties are crucial for successful modeling and

105 forecasting of subsurface fluid flow. Accordingly, several scholars have attempted to overcome
106 these problems by adopting novel techniques such as multilevel–multitracer testing methods and
107 equipment, reactive and nonreactive tracers (e.g., deoxyribonucleic acid molecules), and
108 stochastic simulations (Ptak et al., 2004).

109 This study developed and validated a concept to quantify the heterogeneity of pore
110 distribution associated with subsurface fluid flow based on the novel perspective of combining
111 the pressure and tracer concentration responses obtained during conventional pressure transient
112 and tracer tests, respectively. As discussed earlier, the pressure and tracer concentration
113 responses obey the diffusion and advection–dispersion problems, respectively. This difference in
114 the physical mechanisms yields dissimilar responses to the heterogeneity of the pore distribution.
115 The pressure variations occurring during a pressure transient test propagates throughout a
116 reservoir, regardless of pore geometry, whereas the fluid flow containing a tracer is only
117 generated at a portion of the total pore volume along the flow paths, which avoids the branches
118 and dead ends in a quasi-steady state. Thus, the visible pore volume obtained using the tracer test
119 is limited, whereas the pressure transient test can be employed to investigate the total pore
120 volume. If both visible volumes coincide, the actual pore distribution can be interpreted as
121 homogeneously planar without branches and dead ends. Based on this concept, we defined a
122 scale to quantify the heterogeneity of the pore distribution from a particular aspect: the deviation
123 of the actual pore distribution from a homogeneously planar distribution. This study aimed to
124 elucidate this concept at multiples scales, followed by the validation through laboratory
125 experiments and numerical reservoir simulations. Ultimately, a potential application of the
126 proposed concept has been described for quantifying the existence of permeable structures that
127 remain undiscovered during the exploration and development of reservoirs. Furthermore, this
128 concept enables the assessment of a reservoir simulation model in accurately expressing an
129 actual permeable structure.

130 **2 Concept**

131 2.1 Fracture Network with Branches and Dead Ends

132 Let us consider two schematic examples at distinct scales. In the first case, we consider a
133 portion of a naturally fractured water-dominated reservoir at a relatively small scale of several

meters to several tens of meters (Figure 1a). Generally, permeable fracture networks contain numerous branches and dead ends that generate heterogeneity in the pore distribution (Bisdom et al., 2016; Zuo et al., 2019). For simplicity, the rock matrix was assumed as fully impermeable. Upon performing a pressure transient test using wells intersecting the reservoir, the pressure variation obeying a diffusion problem propagates throughout the fracture network, regardless of the branches and dead ends. By analyzing the pressure responses at the flowing or monitoring wells at the field scale, the total pore volume including the volume of branches and dead ends is quantified and estimated as a storativity value (Horne, 1995; Houzé et al., 2012; Zarrouk & McLean, 2019). Structures equivalent to the branches and dead ends are potentially generated along the fracture surface via nonuniform aperture distribution (Pyrak-Nolte et al, 1988; Sawayama et al., 2021) forming an enclosed space with a narrow entrance. A fault core itself may branch or anastomose, sometimes with branching subsidiary faults (Faulkner et al., 2010).

In general, tracer tests are performed under stable conditions with approximately constant flow rates after an adequate period of time has elapsed since the start of production and reinjection (Fukuda et al., 2005; Kumagai & Kitao, 2000; Rose et al., 2001; Sanjuan et al., 2006), which allows the assumption of a quasi-steady state in a reservoir. Under this condition, the flow paths of the tracer are determined predominantly along the continuous pathways from a reinjection well to production wells, avoiding branches and dead ends (Figure 1a). At a sufficiently smaller time-scale compared with the molecular diffusion toward each branch, tracer concentration responses at the production wells represent only the limited pore volume contributing to the generation of the tracer flow paths. This pore volume can be estimated by analyzing the tracer concentration responses to determine several conventional parameters such as total recovery and residence time (Grant & Bixley, 2011). Alternatively, a more direct and sophisticated approach involves simulating tracer concentration responses by developing a reservoir simulation model that has been successfully applied in multiple fields (Egert et al., 2020; Nakao et al., 2007; Ponte et al., 2009).

Estimated based on pressure responses, storativity can be regarded as the product of the total compressibility and aperture of an equivalent planar fracture (i.e., porosity–thickness product for a porous layer), as demonstrated by Grant and Bixley (2011) for Ohaaki field. Based on the pressure responses, the equivalent planar fracture considers the total pore volume, including the volume of branches and dead ends. Moreover, another equivalent planar fracture

can be determined according to the tracer concentration responses that represent only a portion of the total pore volume covered by a tracer (Figure 1b–c). In case the fracture network contains no branches or dead ends, both apertures coincide to indicate a single planar fracture. Thus, the difference between the apertures of the equivalent planar fractures can be regarded as a scale quantifying the deviation from the homogeneously planar pore distribution, which signifies the heterogeneity of the pore distribution. As portrayed in Figure 1a, flow paths may occasionally include minor bypasses, and accordingly, such bypasses will not contribute toward generating a deviation from the planar pore distribution. Notably, major bypasses that cannot be neglected based on pressure and/or tracer concentration responses are interpreted as multiple planar pore distributions. In the exemplary case of Ohaaki field (Grant & Bixley, 2011), a porosity–thickness product of 300 m was estimated based on the pressure interference at a monitoring well. This is because a single planar reservoir was assumed for analyzing the pressure interference, regardless of the actual three-dimensional reservoir structure (Mroczek et al., 2016).

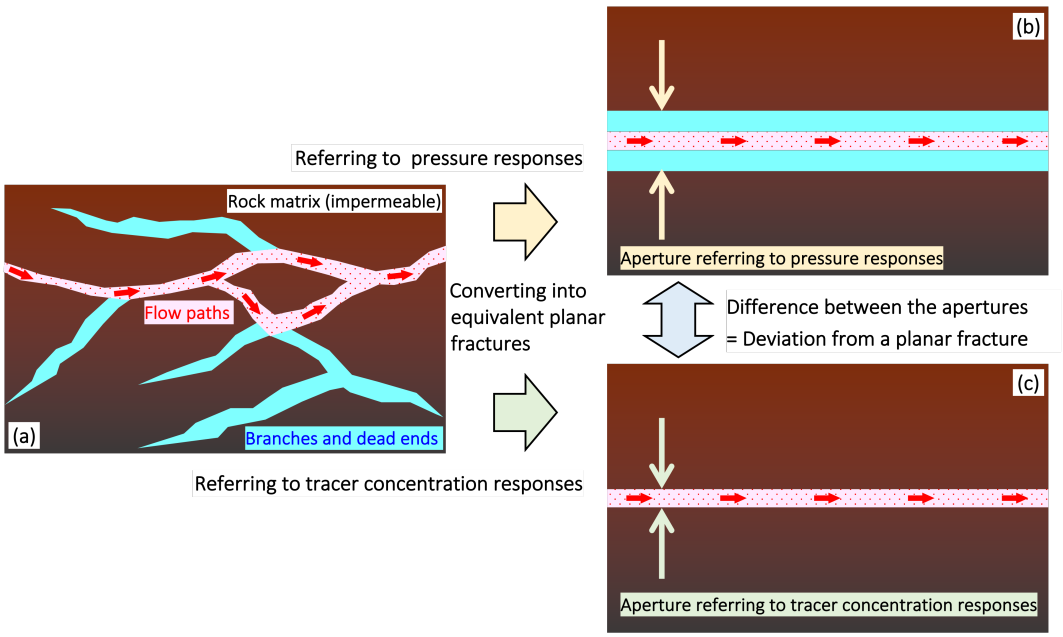

Figure 1. Schematic of a fracture network forming a reservoir and equivalent planar fractures. (a) Heterogeneous pore distribution generated by fracture network contains continuous flow paths as well as branches and dead ends. (b) Aperture of an equivalent planar fracture determined referring to pressure responses represents the total pore volume, because pressure variation propagates throughout the total pore volume. (c) Aperture determined referring to tracer concentration responses represents only a portion of the total pore volume that generates flow

paths. The difference between the apertures quantifies the deviation of the fracture network from a planar fracture.

2.2 Faults Distributed in Parallel

The second case assumes a relatively large scale of several kilometers to consider the total prospect. Let us consider a water-dominated isothermal reservoir with heterogeneous pore distribution generated by parallel-distributed steep faults with stepwise displacement, as described by Bense et al. (2013) and Cole et al. (2005). All the faults were connected to each other through horizontal permeable structures. As described in Figure 2, one of the faults is known through an ongoing exploration, whereas the others remain unknown. Accordingly, pressure transient and tracer tests were performed using production and reinjection wells intersecting a known fault. The pressure variation caused by production and reinjection propagates throughout the reservoir, including the unknown faults. A tracer is injected into the reinjected fluid under quasi-steady-state conditions after a sufficient period of time has elapsed since the start of production and reinjection. In particular, the tracer flow paths are strongly controlled by the fluid flow from the reinjection to the production well through the known fault, because both wells intersect only the known fault. Thus, the tracer concentration response at the production well represents only a portion of the total pore volume generated by a known fault. At this stage of ongoing exploration, reservoir engineers have attempted to analyze the pressure and tracer concentration responses by assuming only a known fault. However, the aperture of an equivalent planar fracture determined from the pressure response is larger than that evaluated using the tracer concentration response.

As discussed earlier, the difference between the apertures of equivalent planar fractures with respect to the pressure and tracer concentration responses indicates a deviation from the planar pore distribution. On a large scale, a difference between the apertures indicates the existence of unknown faults, as observed in the second case. Thus, this difference can act as a potential indicator to quantify the unexplored permeable structures, which will provide us an insightful guide for performing prospective explorations in future. As long as the pressure variation obeys diffusion problems, this indicator is valid for fractured reservoirs as well as for both porous and fractured porous reservoirs.

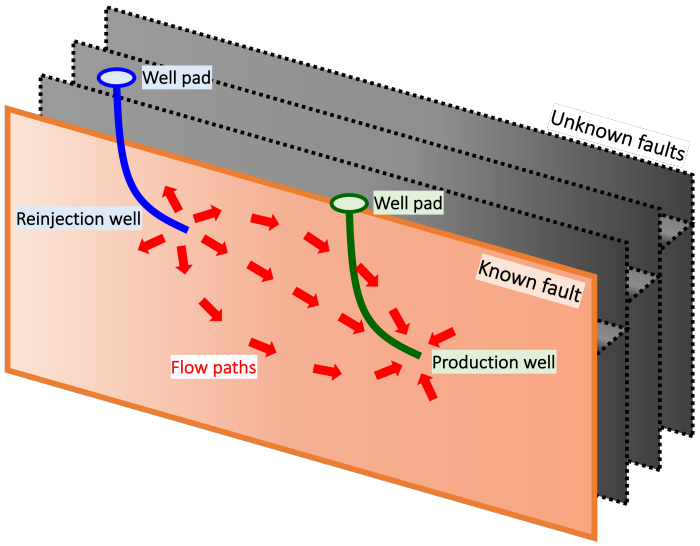

Figure 2. Schematic of parallel-distributed steep faults. Production and reinjection wells are drilled directionally and intersect the known fault only if the other three faults are unknown. All faults are connected through horizontal permeable structures.

3 Laboratory Experiments

The concept described in Section 2 is validated herein. For the first case involving the relatively small scale, we simulated the pressure and tracer concentration responses using laboratory experiments. The experiments were performed assuming a quasi-Hagen–Poiseuille flow in the urethane tube. Based on the experimental results, the original Hagen–Poiseuille flow was modified to account for the additional pressure loss. We aimed to derive a mathematically common diffusion equation with respect to pressure, which will describe the mass conservation in a tube and reservoir as both quasi-Hagen–Poiseuille and Darcy flows contain a common mathematical expression. Overall, the apparent and actual inner diameters of the tube corresponded to the apertures of the equivalent planar fractures discussed in Section 2.

3.1 Apparatus

A schematic of the experimental apparatus assembled under atmospheric pressure and temperature conditions is illustrated in Figure 3. This apparatus was used to generate a flow of tap water under a controlled, constant pressure gradient in a horizontal urethane of 4 mm inner diameter. The pressure gradient was controlled by adjusting the upstream and downstream header tank levels, which were connected to the urethane tube through silicon tubes with a larger

inner diameter of 9 mm to reduce pressure loss. In addition, four diaphragm pressure sensors (PK025SA506, Fuji Controls Co., Ltd.) corresponding to Channels 1–4 were placed along the urethane tube. The pressure sensors produced an output analogue voltage ranging from 0.2–4.6 V, corresponding to a pressure variation of 0.0–25.0 kPaG, recorded at intervals of 1 ms using a high-speed data logger. Prior to the experiments, the voltage values were calibrated and validated to reduce the individual differences between the sensors within 0.024 V (0.13 kPa). Eventually, the flow was generated by opening Valve A placed upstream of the urethane tube.

At the midpoint of the horizontal urethane tube, a cylindrical buffer tank was connected (Figure 3). This tank buffered the transient pressure variations in the horizontal tube. The thickness of air h_{a} in the buffer tank can be adjusted by leveling the buffer tank via closing Valves A, E1, and E2 and opening Valves B, C, D1, and D2. As observed, the water level in the buffer tank corresponded to that in the downstream header tank. Valve C was closed, except for adjusting the air thickness in the buffer tank. As illustrated in Figure 1, we intended to mimic a branch and a dead end by connecting the buffer tank. In addition, the effective volume of the mimicked branch and dead end filled with water could be varied by adjusting the air thickness in the buffer tank. Let us assume that the mixture of water and air in the buffer tank exhibits bulk compressibility $\bar{c}$ and a total volume V. If a variation in this volume of mixture caused by compression is equal to that in the effective volume V' filled with water, the relationship $V'/V = \bar{c}/c_{\mathrm{w}}$ is satisfied, where c_{w} denotes the compressibility of water. The buffer tank can be disconnected by closing Valve B, which mimics a planar fracture without branches or dead ends.

A solution of the tracer Ponceau 4R can be injected into the horizontal tube (Figure 3). At the instant of closing Valves E1 and E2 and opening Valves F1 and F2, the water in the interval between Valves E1 and E2 was replaced with a solution injected with a syringe through Valve F1. Subsequently, the water originally stored in the interval was ejected through Valve F2. The volumetric capacity of the interval was estimated as 3.87 mL based on the inner diameter of the tube (4 mm), length (300 mm), and spacing (8 mm in total) of the connectors. Approximately 10 mL of the solution was injected by referring to the scale on the syringe, and the ejection of red-colored water through Valve F2 was observed. After introducing the tracer solution, it can be injected into the water flowing in the tube by closing Valves D1 and D2 and simultaneously opening Valves E1 and E2. As such, the motions of the four solenoid valves were electrically

synchronized, and three concentration sensors for the tracer were placed near both ends and the midpoint of the horizontal urethane tube.

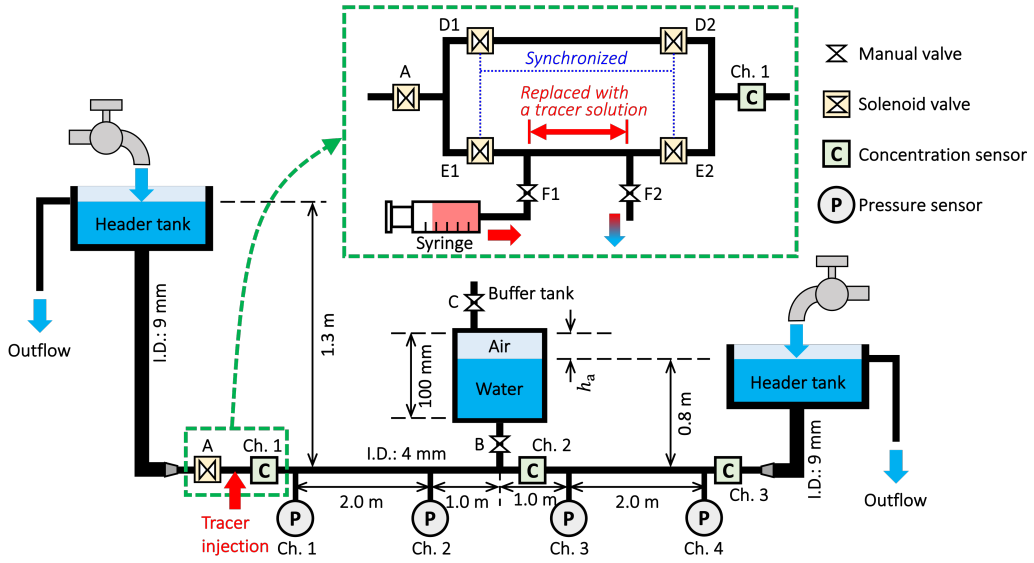

Figure 3. Schematic of experimental apparatus. At the midpoint of the horizontal urethane tube, a buffer tank with an inner diameter of 93 mm and height of 100 mm was connected through another urethane tube with an inner diameter of 4 mm and length of 1.5 m. Water levels in the buffer tank and that in the downstream header tank were maintained identical. The precise distances of the pressure sensors placed in Channels 2–4 from that in Channel 1 were 2.008, 4.024, and 6.032 m, respectively, including the spacings in the connectors. The precise distances of the concentration sensors located in Channels 2 and 3 from that in Channel 1 were 3.325 and 6.238 m, respectively. The distance between the pressure and concentration sensors in Channel 1 was 0.132 m. During the experiments, the ambient pressure and temperature measured in the laboratory were 996.9 hPa and 28.8 °C, respectively.

We designed in-house concentration sensors based on those developed by Takaki et al. (2015). In these sensors, green light with a peak wavelength of 520–525 nm from a light-emitting diode (DiCUNO) was transmitted through the urethane tube and received by a phototransistor (NJL7502L, Nisshinbo Micro Devices Inc.) with a peak sensitivity wavelength of 560 nm. As the peak absorbance wavelength of the tracer Ponceau 4R was 508 nm (Bevziuk et al., 2017), the voltage between a resistor connected to the emitter of the phototransistor varied sensitively depending on the tracer concentration in the water flowing in the tube. The

relationship between the concentration C_n [wt%] for Channel n and voltage V [V] was calibrated for each sensor using reference solutions prepared with multiple concentrations. The relationships were summarized using the following empirical expressions (Table 1, Figure 4):

$$\log C_n = a_n + b_n \log V + c_n (\log V)^2 + \frac{d_n}{\log V - \log V_{0n}}, \quad (1)$$

where a_n, b_n, c_n, and d_n denote constants, and V_{0n} [V] indicates the voltage of pure water. The constants were determined using the least-squares method implemented.

Table 1

Constants for Equation 1

n	a_n	b_n	c_n	d_n	$\log V_{0n}$
1	−1.45790	−1.40794	0.634143	0.00105583	0.681784
2	−1.81174	−1.09609	0.661727	0.000914718	0.678973
3	−1.55684	−1.35305	0.679273	0.000940129	0.680879

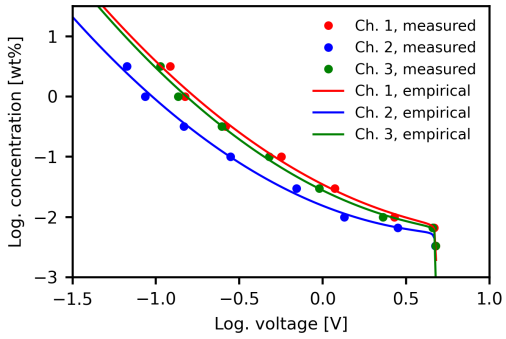

Figure 4. Relationship between tracer concentration and output voltage for each concentration sensor. Empirical relationships obey Equation 1 with the constants summarized in Table 1.

3.2 Conditions and Results

Four experiments were performed using various conditions of the buffer tank. In the first experiment, the buffer tank was disconnected, whereas the remaining experiments were performed by connecting the buffer tank with air thicknesses of 17, 28, and 39 mm. The water

299 levels of the upstream and downstream header tanks were set at 1.3 and 0.8 m, respectively,
300 above the horizontal urethane tube (Figure 3). Under steady-state conditions with this pressure
301 gradient, the volumetric flow rate in the horizontal tube was determined in advance by measuring
302 the overflow from the downstream header tank as 141.26 mL min^{-1} at no water supply to the
303 downstream header tank. This value represents the average of ten measurements with a standard
304 deviation of 1.6%. Prior to each experiment, the water originally stored in the interval between
305 Valves F1 and F2 was replaced with a tracer solution (0.5 wt %).

306 The experiments were performed using a common procedure. In the initial state, Valves
307 A, C, E1, E2, F1, and F2 were closed, whereas Valves D1 and D2 were open. The state of Valve
308 B varied depending on the experiment. First, the transient pressure response was measured after
309 opening Valve A. The pressure monitored at each sensor converged to a constant value after a
310 few tens of seconds at most after opening Valve A, which indicated a steady state. After 110 s of
311 opening Valve A, the tracer was injected by opening Valves E1 and E2, and closing Valves D1
312 and D2. The tracer concentration response was measured for 90 s after tracer injection. The
313 precise time of opening Valve A and injecting the tracer could be determined from the pressure
314 data that recorded noise caused by the motions of the values.

315 The pressure responses during the four experiments are presented in Figure 5. All
316 responses initially exhibited noise with relatively high frequencies, which was caused by the
317 motion of Valve A during opening. After the noise ceased, monotonous variations were
318 observed, during which the pressure variations differed with the buffer tank conditions. Without
319 the buffer tank (Figure 5a), the pressure response in each channel varied steeply. As the buffer
320 tank was connected (Figure 5b–d), the pressure responses became more gradual with increasing
321 air thickness h_a in the buffer tank. The pressure responses for all the experiments ultimately
322 reached a common steady state, independent of the buffer tank condition. The tracer
323 concentration responses are presented in Figure 6. All responses exhibited a steep variation at the
324 upstream point (Channel 1), followed by gradual variations at the downstream points (Channels
325 2 and 3) because of mechanical dispersion. Remarkably, none of the tracer concentration
326 responses exhibited an apparent dependence on the buffer tank condition.

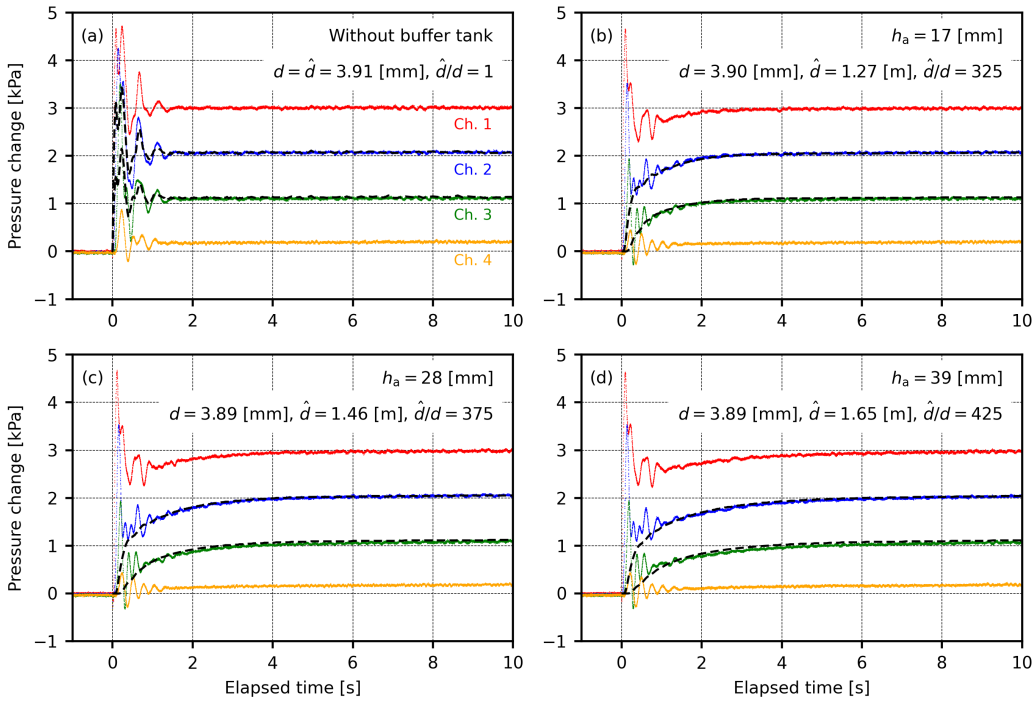

Figure 5. Pressure responses after opening Valve A for four buffer tank conditions. (a) Buffer tank was disconnected. (b)–(d) Air thickness h_a in the buffer tank was modified from 17 to 39 mm. Red, blue, green, and orange plots indicate experimental observations at the sensors for Channels 1–4, respectively. Broken lines indicate numerical solutions of Equation 2. Estimated values of apparent tube inner diameter $\hat{d}$ and the ratio of that to the actual inner diameter $\hat{d}/d$ are

noted for each experiment. Values of actual inner diameter d were estimated from tracer concentration responses (Figure 6).

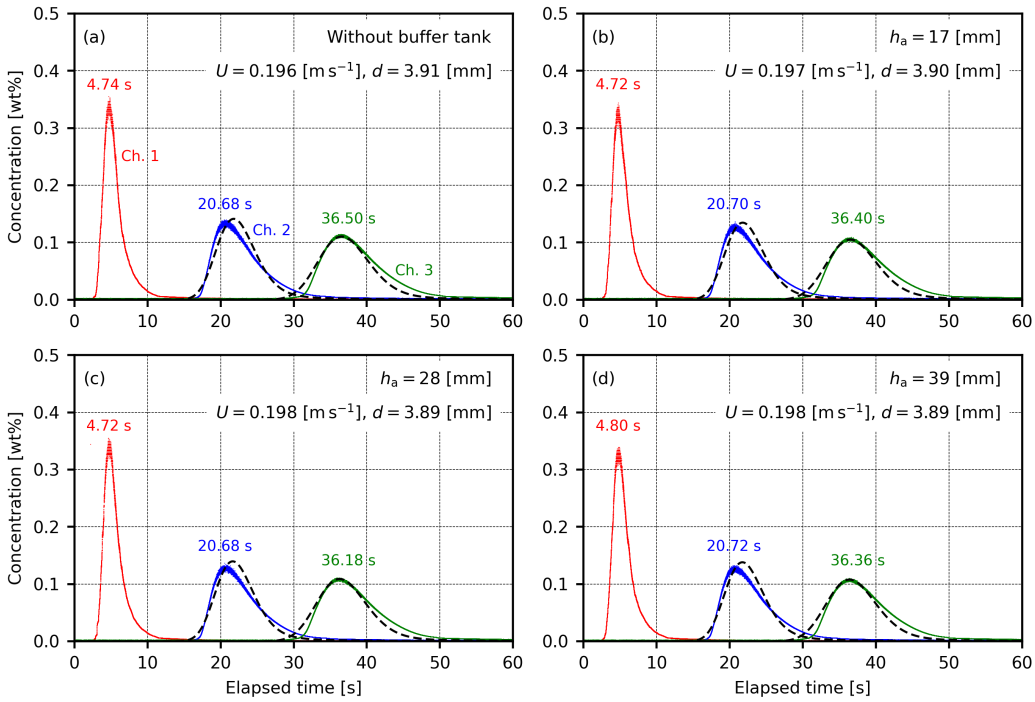

Figure 6. Tracer concentration responses after tracer injection in four buffer tank conditions. (a) Disconnected buffer tank. (b)–(d) Air thickness h_a in buffer tank was modified from 17 to 39 mm. Red, blue, and green plots indicate experimental observations at sensors for Channels 1–3, respectively. Broken lines indicate numerical solutions of Equation 3. The observed peak time for each sensor as well as the estimated flow velocity U and tube inner diameter d are presented for each experiment.

3.3 Discussion

The concept described in Section 2 is experimentally validated herein. Assuming a quasi-Hagen–Poiseuille flow of water with compressibility c_w and viscosity μ in the horizontal urethane tube with the actual inner diameter d, we obtain the following diffusion equation with respect to the pressure P depending on time t and distance x along the tube based on mass conservation:

$$c_{\mathrm{w}}\hat{d}^2\frac{\partial P}{\partial t} = a\frac{d^4}{32\mu}\frac{\partial^2 P}{\partial x^2}, \tag{2}$$

where a and $\hat{d}$ are the modification factor and apparent inner diameter of the tube, respectively. The apparent inner diameter $\hat{d}$ of the tube can vary from the actual inner diameter d depending on the condition of the buffer tank. Considering the flow in a single tube, $\hat{d} = d$. The modification factor a is factored to modify the original Hagen–Poiseuille flow to correspond to the experimental results, including the additional pressure loss. Furthermore, we obtain the advection–dispersion equation with respect to the tracer concentration C in the horizontal tube as follows:

$$\frac{\partial C}{\partial t} + U\frac{\partial C}{\partial x} = D\frac{\partial^2 C}{\partial x^2}, \tag{3}$$

where, U and D are the flow velocity and dispersion coefficient, respectively. Under steady-state conditions in the experiments, the flow velocity U is determined as $U = 4Q/(\pi d^2)$, where Q denotes the volumetric flow rate.

Assuming a single tube, we initially determined the flow velocity and inner diameter of the horizontal urethane tube according to the tracer concentration responses (Figure 6) and the volumetric flow rate measured prior to the experiments. The flow velocity was determined from the observed peak instant and the distance for each concentration sensor using linear regression. The inner diameter of the tube was determined from the flow velocity and volumetric flow rate. As summarized in Figure 6, the flow velocity and inner diameter of the tube were independent of the buffer tank condition. The inner diameter of the tube was estimated at approximately 4 mm, which is consistent with the specifications provided by the manufacturer. In particular, the connection to the buffer tank did not affect advection and dispersion in the horizontal tube.

The broken lines in Figure 6 represent the numerical solutions of Equation 3 using the estimated flow velocity value U for each experiment. The value of the dispersion coefficient D was commonly assumed as 6.0×10^{-3} m^2 s^{-1} for correspondence between the simulations and observations. We adopted a combined numerical technique of the constrained interpolation profile method (Yabe et al., 1991; Yabe & Aoki, 1991) to reduce numerical dispersion for the advection term and the conventional explicit finite difference method for the dispersion term. The grid sizes for temporal and spatial discretization were 1.0×10^{-4} s and 1.0×10^{-2} m,

respectively. For the upstream boundary condition, we assumed the temporal variations observed at the sensor located in Channel 1. In addition, an outflow boundary was assumed for the downstream boundary condition at the location of the sensor in Channel 3. The numerical solutions validated the consistency of the experimental results with the theoretical solution of the one-dimensional advection–dispersion problem (Equation 3).

Subsequently, we interpreted the pressure responses (Figure 5) in terms of the one-dimensional diffusion problem (Equation 2). The broken lines in Figure 5 indicate the numerical solutions to Equation 2, which were obtained assuming the actual inner diameter d of the tube based on the tracer concentration response observed in each experiment (Figure 6). The compressibility c_{w} and viscosity μ of water were assumed as 5.1210×10^{-10} [Pa^{-1}] and 8.1823×10^{-4} [Pa s], respectively, referring to the measured ambient pressure and temperature as well as the empirical equations developed by the International Association for the Properties of Water and Steam (IAPWS) (IAPWS, 1997, 2007). The volumetric flow rate estimated by assuming these parameter values and the Hagen–Poiseuille flow was less than that measured prior to the experiments (141.26 mL min^{-1}), implying additional pressure loss. To compensate this inconsistency, we adopted a quasi-Hagen–Poiseuille flow containing a modification factor a, ranging from 0.72–0.74, as expressed in Equation 2. The additional pressure loss was potentially generated by the connectors for the pressure sensors and buffer tank as well as the loop-shaped horizontal urethane tube with a diameter of ~0.3 m. The values of the Reynolds number determined from the conditions of these experiments ranged from approximately 930–940, which are less than the critical value of 1800 (Landau & Lifshitz, 1987) for the transition between laminar and turbulent flows. We adopted the conventional implicit finite difference method to solve Equation 2 numerically. To simulate a pressure response for 10 s, the temporal grid size expanded exponentially from 1.0×10^{-9} to 1.5×10^{-3} s, and the spatial grid size was uniform at 1.0×10^{-2} m. The boundaries with temporally varying pressures were assumed according to the variations observed at the sensors located in Channels 1 and 4.

Under the above conditions, the pressure variations observed at the sensors placed in Channels 2 and 3 during each experiment were simulated in series, and the ratio of the tube inner diameter $\hat{d}/d$ was altered to ensure correspondence between the simulations and observations. As depicted in Figure 5, the simulations with the best-fit value of $\hat{d}/d$ successfully reproduced

all the experimental observations, including that without the buffer tank ($\hat{d}/d = 1$). Depending on the effective volume of the water-filled buffer tank, the connection of the buffer tank, such as that in the experiments, is equivalent to assuming an apparent tube inner diameter $\hat{d}$ several hundred times larger than the actual value d. This implies that the difference between the apparent and actual inner diameters quantifies the deviation from a single tube. Compared with the diffusion equation with respect to reservoir pressure (Zarrouk & McLean, 2019), the factors $c_{\mathrm{w}}\hat{d}^2$ and $ad^4/32\mu$ in Equation 2 correspond to the storativity and transmissivity of a reservoir, respectively. Based on the experimental results, we conclude that an increase in the volume of branches and dead ends (Figure 1) mimicked using the buffer tank (Figure 3) can be quantitatively indicated by the apparent increase in storativity, which is defined as the product of the total compressibility and aperture of an equivalent planar fracture. Assuming a total compressibility value based on the realistic values for fluids and formations, the increase in storativity can be interpreted as an increase in the aperture of an equivalent planar fracture. Alternatively, the aperture of an equivalent planar fracture can be independently estimated from the tracer concentration responses, such as that in the experiments (Figure 6), which only represents a portion of the total pore volume and is unaffected by the branches and dead ends. Thus, based on the pressure and tracer concentration responses, the deviation from the planar pore distribution containing no branches or dead ends can be quantified in terms of the difference between the apertures of equivalent planar fractures, as described in Section 2. Further quantitative discussions regarding the pore volume are presented in Section 5.

4 Reservoir Simulations

The concept described in Section 2 was validated at a relatively large scale using numerical reservoir simulations. As discussed earlier, we assumed a known vertical fault and unknown permeable structures such as faults or a porous layer. The unknown permeable structures were connected to the known fault. The pressure transient and tracer tests were performed using production and reinjection wells that intersected only the known fault. Accordingly, the pressure and tracer concentration responses were investigated under several conditions of unknown permeable structures.

4.1 Conditions

The two models used for the numerical reservoir simulations are presented in Figure 7. Both models assumed a known vertical fault with a vertical dimension of 2.0 km. Assuming an extremely large horizontal dimension of 2000 km, we intended to place infinite-acting boundary conditions. The first model assumed that the vertical unknown faults were distributed parallel to the known fault (Figure 7a), and the vertical and horizontal dimensions of the unknown vertical faults were identical to those of the known faults. The spacing between the known and unknown faults was uniform at 0.4 km, and all faults were connected at 0.4 km from the upper boundary through a horizontal permeable structure. The second model assumed an unknown horizontal porous layer (Figure 7b). The dimensions of the unknown porous layer in the direction perpendicular to the known fault ranged several kilometers, whereas that parallel to the known fault was 2000 km, as assumed for the known fault. The unknown porous layer intersected the known fault at 0.4 km from the upper boundary. The production and reinjection wells intersected the known fault at the vertical middle points with a spacing interval of 1.0 km. The production and reinjection flow rates were constant at 200 and 160 t h^{-1}, respectively. Subsequently, a tracer was injected into the reinjected fluid after 10 to 11 d since the start of production and reinjection. The tracer concentration in the reinjected fluid was maintained at 10 ppm.

The numerical simulations were performed using the code developed by Matsumoto (2020). The code based on the finite difference method can develop a single-phase and non-isothermal discrete-fracture network model, including conductive heat transfer in the direction perpendicular to each fracture. The pressure responses at the flowing wells were accurately simulated using highly refined local grids that accurately simulated the steep pressure variations in the vicinity of the flowing wells. To effectively reduce numerical dispersion, the flows of the tracer were simulated using the constrained interpolation profile method (Yabe et al., 1991; Yabe & Aoki, 1991). The thermodynamic properties and viscosity of water were computed using the empirical equation developed by the IAPWS (IAPWS, 1997, 2007). Using this code, a two-dimensional Cartesian spatial grid was defined for each planar permeable structure (Figure 7). The grid size of the vertical faults in the vertical direction was 100 m. In particular, the horizontal direction varied depending on the region. In the inner region (3.0 km from the reinjection well toward both sides), the grid size was uniform at 100 m. In the outer regions, the grid size expanded exponentially from 100 m to 250 km. Moreover, the grid size for the

horizontal permeable structure (Figure 7a) in the direction perpendicular to the vertical faults was 100 m. In contrast, the grid size for the unknown porous layer (Figure 7b) in the direction perpendicular to the vertical fault varied from 100 m to 1.17 km at most, depending on the dimension L. For both the horizontal permeable structure (Figure 7a) and the unknown porous layer (Figure 7b) in the direction parallel to the vertical faults, the grid sizes were identical to those for the vertical faults. The temporal grid size expanded exponentially from 6.61×10^{-8} s after four days from starting production and reinjection, followed by a constant value of 4.74×10^{-1} h.

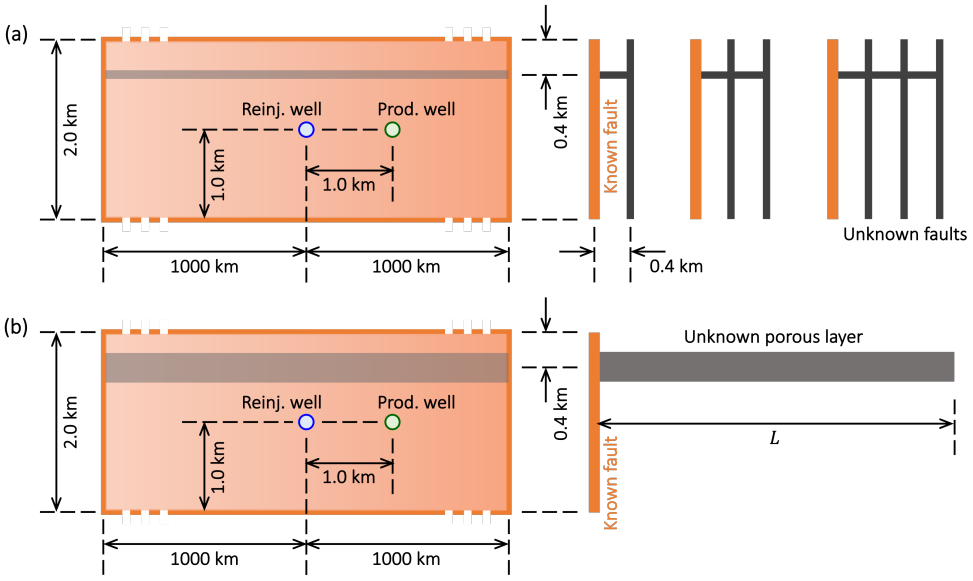

Figure 7. Reservoir simulation models. The known vertical fault is connected with (a) unknown faults in parallel or (b) an unknown porous layer. The extremely large horizontal dimension of 2000 km represents infinite-acting boundary conditions. The upper and lower boundaries as well as the boundary along the unknown porous layer on the opposite side of the known fault are impermeable. Under a natural state, the reservoir pressure follows a hydrostatic pressure distribution of 12 MPa at 0.4 km from the upper boundary. The specific enthalpy is uniform at 1085.8 kJ kg^{-1} (i.e., approximately uniform temperature distribution at 250 °C). The physical properties of the faults and porous layer are uniform and constant. The permeability–thickness product is 1.0×10^{-11} m^3. Porosity–thickness product is 2.0×10^{-1} m, except the unknown

porous layer that is assumed as 1.0 m. The dispersion coefficient for the tracer is 1.0×10^{-2} m^2 s^{-1}.

4.2 Results and Discussion

The pressure responses at the production well for both the models are depicted in Figure 8, assuming the unknown faults and porous layer in terms of drawdown ΔP and its derivative $\partial \Delta P / \partial (\ln t) = t \, \partial \Delta P / \partial t$, where t denotes the time elapsed since the start of production and reinjection. As conventionally adopted in the well test analysis (Houzé et al., 2012), the pressure responses can be interpreted as a superposition of those for two problems: production and reinjection at the same rate of 160 t h^{-1} and production at a rate of 40 t h^{-1} without reinjection. As observed, the pressure response component obeying the former problem converged to a steady state that depends solely on transmissivity. In contrast, the latter problem represents production at a constant rate that generates a linear flow depending solely on the product of the transmissivity and storativity (Gringarten et al., 1974). Upon combining these two problems, we can ensure that the pressure response independently relies on transmissivity and storativity.

The variations of the apparent porosity–thickness product of the known fault (i.e., aperture of an equivalent planar fracture) after connection to the unknown faults or porous layer are depicted in Figure 8. After coinciding with the original value of the known fault at the initial time interval, the apparent porosity–thickness product gradually increased and converged to a specific value depending on the conditions of the unknown permeable structures. Referring to the straight lines with a slope of 0.5 determined from the derivative, the predominance of the linear flow can be observed (Gringarten et al., 1974). According to the conditions of the unknown permeable structures, the apparent porosity–thickness product varied by orders of magnitude. For the model assuming one to three unknown faults, the apparent porosity–thickness products were $10^{0.668}$ (= 4.66), $10^{1.04}$ (= 11.0), and $10^{1.30}$ (= 19.8) times larger than the original value, respectively. Assuming an unknown porous layer with dimensions of 4, 8, and 12 km, the apparent porosity–thickness products were $10^{1.50}$ (= 31.8), $10^{2.00}$ (= 100), and $10^{2.31}$ (= 205) times larger, respectively.

Similar to the pressure responses, the tracer concentration responses for both the models are illustrated in Figure 9 along with the reference responses. The tracer concentration responses indicated an apparent porosity–thickness product that was ~$10^{0.1}$ (= 1.26) times larger than the

original value of the known fault, with a low dependence on the conditions of the unknown permeable structures. This slightly larger value of the apparent porosity–thickness product resulted from the transfer of the tracer via dispersion from the known fault to the unknown permeable structures. For simplicity, the dispersion coefficient in this numerical model was assumed to be constant, although certain sophisticated models often assume smaller values with lower flow velocities (Bear, 1972, 1979). In case of the predominant flow from the reinjection well to the production well only through the know fault, the transfer of the tracer from the known fault to the unknown permeable structures was potentially overestimated. In case of adopting the values in this study, the apparent porosity–thickness products derived from the tracer concentration responses could adequately reproduce the original value of the known fault, regardless of the unknown permeable structures. Based on the tracer concentration responses, the apparent variation in the porosity–thickness product was orders of magnitude less than that derived from the pressure responses depending on the condition of the unknown permeable structures. Thus, the results of the numerical reservoir simulations signify that the deviation of a three-dimensional reservoir structure from an assumed single planar reservoir (i.e., known fault) can be quantified based on the difference between the apertures of equivalent planar fractures (i.e., apparent porosity–thickness products) with respect to pressure and tracer concentration responses, as described in Section 2.

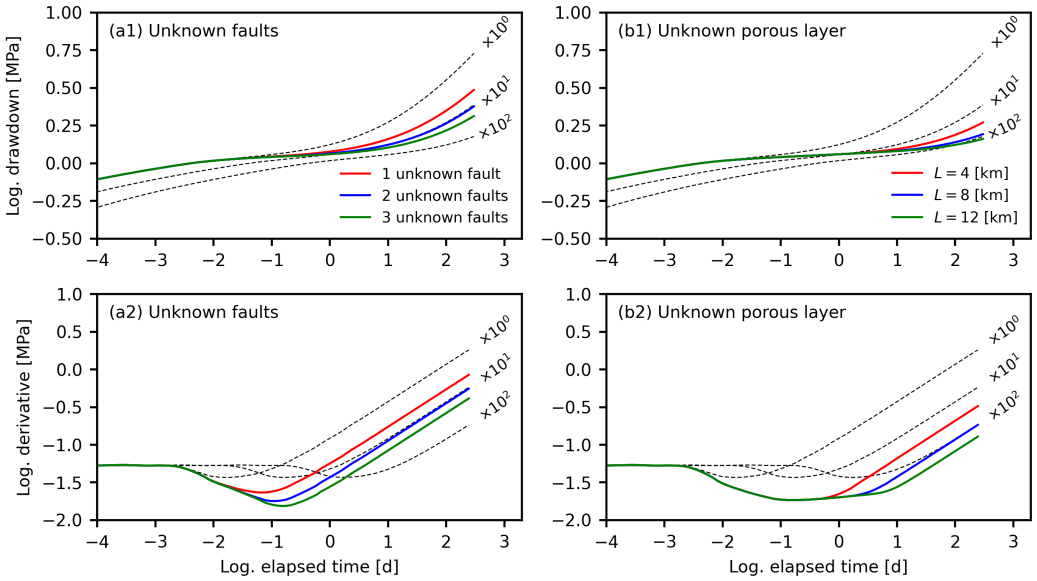

Figure 8. Pressure responses at production well after the initiation of production and reinjection for several conditions of unknown permeable structures: variations in drawdown and its derivative assuming one to three unknown faults (a1, a2) and those assuming an unknown porous layer with a dimension of 4 to 12 km (b1, b2). The responses associated with the unknown permeable structures (solid lines) were superimposed on the reference responses, assuming only the known fault with the original porosity–thickness product value, 0.2 m, multiplied by three factors (broken lines).

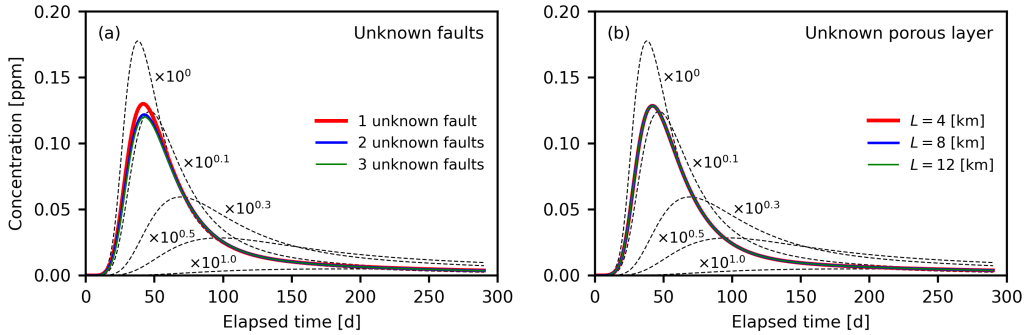

Figure 9. Tracer concentration responses at production well after injection, ten days after starting production and reinjection, for several conditions of the unknown permeable structures: one to three unknown faults (a1, a2) and an unknown porous layer with a dimension of 4 to 12 km (b1, b2). The responses associated with the unknown permeable structures (solid lines) are superimposed on the reference responses assuming the known fault only with the original porosity–thickness product value, 0.2 m, multiplied by five factors (broken lines).

5 Discussion

5.1 Relationship between Apparent and Actual Pore Volumes

The connection of the unknown buffer tank or permeable structures increased the apparent volumetric capacity of the known tube or fault, respectively, which were estimated from the pressure responses. We then investigated the relationship between the apparent and actual pore volumes (Figure 10). The actual pore volume for the experiments described in Section 3 was determined by estimating the effective volumetric capacity of the buffer tank, $V' = \bar{c}V/c_{\mathrm{w}}$, filled with water. The mixture of water and air in the buffer tank bears a volume V and bulk compressibility $\bar{c}$, and c_{w} denotes the compressibility of water. To compute the effective

553 volume V', the thermodynamic properties of water and air were referred from IAPWS (2007) and
554 Lemmon et al. (2000), respectively. The volumetric capacity of the tube connecting the buffer
555 tank and horizontal tube was considered as well. The actual pore volume per unit length was
556 determined by dividing the total effective volume by the length of the horizontal tube, including
557 the buffer tank and tubes. The actual pore volume per unit length for the reservoir simulation
558 models was determined by dividing the total pore volume, including the known fault and
559 unknown permeable structures (i.e., unknown faults or porous layer), with the length of the
560 reservoir in the horizontal direction along the known fault. In Figure 10, the apparent pore
561 volume estimated from the pressure responses were compared with the actual pore volume for
562 both the laboratory experiments and reservoir simulations described in Sections 3 and 4.

563 Notably, the apparent pore volume tended to be larger than the actual pore volume
564 (Figure 10), implying that the aperture of an equivalent planar fracture referring to pressure
565 responses during pressure transient tests included excess pore volume. The relationship between
566 the apparent and actual pore volumes determined from the reservoir simulations exhibited
567 straight lines with a slope of 2.0. This indicated that the apparent pore volume was proportional
568 to the square of the actual pore volume. This specific feature provides an insightful guide to
569 reveal the mechanism generating excess pore volume. For the reservoir simulations described in
570 Section 4, the distance between the known fault and the farthest point in the unknown permeable
571 structure in the direction perpendicular to the known fault increased proportionally with the
572 actual pore volume of the unknown permeable structure. After the propagation of pressure
573 variation caused by the production and reinjection reached the farthest point, the pressure
574 response at the production well transitioned to that representing the linear flow, i.e., a straight
575 line with a slope of 0.5 (Figure 8a2 and 8b2). As clarified by the radius of investigation in the
576 well test analysis (Houzé et al., 2012), the time elapsed is proportional to the square of the
577 distance reached by the propagating pressure variation from a source. The reference lines
578 described in Figure 8a2 and 8b2 indicate that the apparent porosity–thickness product (i.e.,
579 apparent pore volume) increased proportionally with the delay, as the straight line appeared.
580 Thus, the apparent pore volume was proportional to the square of the actual pore volume (Figure
581 10). From a general perspective, the excess pore volume is generated by the delay in pressure
582 responses caused by the propagation of pressure variations in the reservoir, independent of
583 reservoir geometry. The relationship between the apparent and actual pore volumes determined

584 from laboratory experiments did not exhibit a straight line with a slope of 2.0, because the
585 distance between the horizontal tube and the farthest point in the buffer tank did not vary with
586 the actual pore volume.

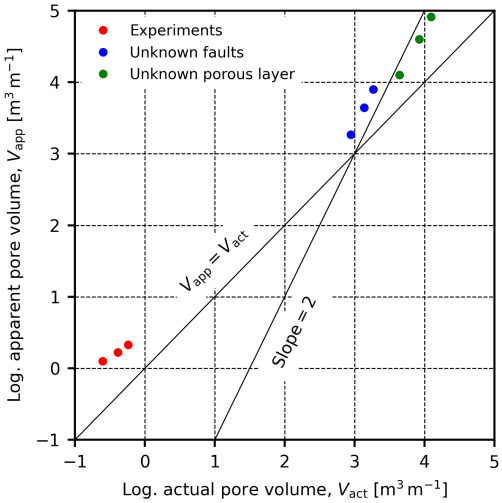

587

588 **Figure 10**. Relationship between apparent and actual pore volumes derived from laboratory
589 experiments (red circles) in Section 3 and reservoir simulations (blue and green circles) in
590 Section 4.

591 5.2 Potential Applications to Geothermal Exploration and Development

592 Let us consider a potential application of the concept, validated in this study, to
593 explorational and developmental project at a geothermal prospect associated with a
594 heterogeneous pore distribution generated by multiple faults. As such, the typical procedure for
595 exploration and development has been established in several textbooks (DiPippo, 2016; Grant &
596 Bixley, 2011): ground surveys based on several geosciences, followed by explorational drilling,
597 production testing, including pressure transient and tracer testing, and reservoir modeling. The
598 proposed concept can be applied to interpret the data obtained from pressure transient and tracer
599 tests performed during production. This enables us to quantitatively assess the existence of
600 permeable structures that have not been considered in the reservoir simulation model. The
601 current model is three-dimensional, practically sophisticated, and constructed based on the
602 results of previous surveys, drilling, and tests. As such, an accurate prediction of unknown
603 permeable structures substantiates further surveys and drilling. This assessment will provide an
604 insightful guide for decision-making, such as advancing to the developmental phase, continuing

exploration, or suspending a project. The possible dimensions and locations of unknown permeable structures can be estimated by constructing a reservoir simulation model, including assumed unknown permeable structures, to match the apertures of equivalent planar fractures based on pressure and tracer concentration responses. To more realistically render the model, the results of geological and geophysical surveys and their interpretations provide useful references for constructing and brushing up the model. Adequate observation and understanding of thermodynamic reservoir conditions are crucial because the bulk compressibility of water increases by four orders of magnitude owing to boiling (Grant & Bixley, 2011), which will potentially lead to an overestimation of the aperture of an equivalent planar fracture referring to pressure responses.

Furthermore, the proposed concept enables us to assess the accuracy of a reservoir simulation model at a relatively small scale. Despite several sophisticated and state-of-the-art modeling techniques (Viswanathan et al., 2022) and progress in computational capacity, we cannot avoid simplifying field observations to a greater or lesser extent during modeling. Let us assume that a field-scale model contains a permeable plane representing a fault confirmed from explorational wells (Figure 7). Even if multiple minor lost-circulation depths and/or drilling breaks exist at a considerable depth interval associated with the main lost-circulation depth, we often expressed a fault using a single plane for simplicity. Referring to the concept as well as the pressure and tracer concentration responses observed during pressure transient and tracer tests, respectively, we will be able to assess the accuracy of the model in expressing the actual permeable structure. If the aperture of an equivalent planar fracture referring to the pressure responses coincides with that referring to the tracer concentration responses, the fault comprises a single planar fracture. Otherwise, minor permeable structures are associated with or intersect the main fault. Remarkably, the application of the concept does not require special methods, techniques, or tools for field tests or modeling. Thus, this concept can be immediately applied to existing observational data obtained from conventional testing methods, adopting conventional reservoir simulators capable of simulating pressure and tracer concentration responses.

6 Conclusions

This study proposed a novel concept to quantify the deviation of the heterogeneous pore distribution associated with branches and dead ends from a planar distribution. At a larger scale,

635 the deviation of a three-dimensional reservoir structure from a planar reservoir can be quantified
636 using this concept. Primarily, the difference between the apertures of the equivalent planar
637 fractures estimated from the pressure and tracer concentration responses during the pressure
638 transient and tracer tests, respectively, forms the key parameter of evaluation. In principle, this
639 concept is based on the variations between physical mechanisms in a heterogeneous pore
640 distribution. The pressure responses obey the diffusion problem, whereas the tracer concentration
641 responses obey the advection–dispersion problem.

642 The proposed concept was validated through laboratory experiments using quasi-Hagen–
643 Poiseuille flow in a urethane tube. A buffer tank mimicking a branch and dead end was
644 connected to the tube midpoint. The apparent inner diameter of the tube, determined from the
645 pressure responses, varied up to 425 times larger than the actual value, depending on the buffer
646 tank condition. Nonetheless, the tracer concentration responses could be independently
647 reproduced by assuming an approximate actual inner diameter, regardless of the buffer tank
648 condition. The difference between the apparent and actual inner diameters varied with the
649 effective volume of the buffer tank, and the deviation from a single tube was successfully
650 quantified.

651 Furthermore, the concept was validated on a larger scale using reservoir simulations,
652 assuming a known fault and unknown permeable structures (i.e., unknown faults or a porous
653 layer). Specifically, the pressure and tracer concentration responses were simulated assuming
654 production and reinjection wells intersecting only the known fault. The apparent porosity–
655 thickness product (i.e., aperture of an equivalent planar fracture) determined from the pressure
656 responses varied up to 205 times larger than the actual value of the known fault, depending on
657 the condition of the unknown permeable structures. Overall, the tracer concentration responses
658 could be reproduced by assuming an approximate actual porosity–thickness product, regardless
659 of the condition of the unknown permeable structures. The difference between the apparent and
660 actual porosity–thickness products varied with the volume of the unknown permeable structures
661 and successfully quantified the deviation from a single fault.

662 The apparent pore volume estimated from the pressure responses tended to be larger than
663 the actual value owing to the delay in pressure responses. In general, a delay is caused when the
664 pressure variation propagates through the pore. This implies that the aperture of an equivalent

665 planar fracture, determined from pressure transient tests, includes an excess pore volume beyond
666 the actual reservoir pore volume. The concept will provide a useful guide for successful
667 explorational and developmental geothermal projects by quantifying the existence of
668 undiscovered permeable structures in a reservoir simulation model. In addition, this concept
669 provides a scale for assessing a reservoir simulation model in accurate expression of an actual
670 heterogeneous permeable structure.

671 **Acknowledgments**

672 We thank Ms. Sora Hanada from Chikushigaoka High School for supporting the
673 reproducibility of the laboratory experiments by performing supplementary experiments as a
674 participant in the QURIES program conducted by Kyushu University. This study was supported
675 by JSPS KAKENHI (Grant Number JP20K05402). We declare that the authors have no known
676 conflicting financial interests or personal relationships that could have appeared to influence the
677 study reported in this paper.

678 **Open Research**

679 The data, including the image files, experimental results, numerical input/output data, and
680 source codes, presented in each figure and table are available at the repository provided by
681 HYDROSHARE via http://www.hydroshare.org/resource/3b66eb5ff9be4dc19d5e726bf4e08cc7
682 (Matsumoto, 2022).

683 **References**

684 Acuna, J. A., & Yortsos, Y. C. (1995). Application of fractal geometry to the study of networks of
685 fractures and their pressure transient. *Water Resources Research*, *31*(3), 527–540.
686 https://doi.org/10.1029/94wr02260

687 Adams, M. C., & Davis, J. (1991). Kinetics of fluorescein decay and its application as a geothermal
688 tracer. *Geothermics*, *20*(1–2), 53–66. https://doi.org/10.1016/0375-6505(91)90005-G

689 Agarwal, R. G., Al-Hussainy, R., & Ramey, H. J. (1970). An investigation of wellbore storage and skin
690 effect in unsteady liquid flow. 1. Analytical treatment. *Society of Petroleum Engineers Journal*,
691 *10*(3), 279–290. https://doi.org/10.2118/2466-pa

692 Al-Hussainy, R., Ramey, H. J., & Crawford, P. B. (1966). The flow of real gases through porous media.

Journal of Petroleum Technology, *18*(5), 624–636. https://doi.org/10.2118/1243-A-PA

Barenblatt, G. I., Zheltov, Iu. P., & Kochina, I. N. (1960). Basic concepts in the theory of seepage of homogeneous liquids in fissured rocks [strata]. *Journal of Applied Mathematics and Mechanics*, *24*(5), 1286–1303. https://doi.org/10.1016/0021-8928(60)90107-6

Bear, J. (1972). Dynamics of fluids in porous media. *Environmental Science Series*. New York, NY: American Elsevier Publishing Co.

Bear, J. (1979). Hydraulics of groundwater. *McGraw-Hill Series in Water Resources and Environmental Engineering* (V. T. Chow, R. Eliassen, & R. K. Linsley, Ed.). New York, NY: McGraw-Hill.

Bense, V. F., Gleeson, T., Loveless, S. E., Bour, O., & Scibek, J. (2013). Fault zone hydrogeology. *Earth-Science Reviews*, *127*, 171–192. https://doi.org/10.1016/j.earscirev.2013.09.008

Bevziuk, K., Chebotarev, A., Snigur, D., Bazel, Y., Fizer, M., & Sidey, V. (2017). Spectrophotometric and theoretical studies of the protonation of Allura Red AC and Ponceau 4R. *Journal of Molecular Structure*, *1144*, 216–224. https://doi.org/10.1016/j.molstruc.2017.05.001

Bisdom, K., Bertotti, G., & Nick, H. M. (2016). The impact of in-situ stress and outcrop-based fracture geometry on hydraulic aperture and upscaled permeability in fractured reservoirs. *Tectonophysics*, *690*, 63–75. https://doi.org/10.1016/j.tecto.2016.04.006

Bourdet, D., Whittle, T. M., Douglas, A. A., & Pirard, Y. M. (1983). A new set of type curves simplifies well test analysis. *World Oil*, *196*(6), 95–101.

Chang, J., & Yortsos, Y. C. (1990). Pressure-transient analysis of fractal reservoirs. *SPE Formation Evaluation*, *5*(1), 31–38. https://doi.org/10.2118/18170-PA

Chrysikopoulos, C. V. (1993). Artificial tracers for geothermal reservoir studies. *Environmental Geology*, *22*(1), 60–70. https://doi.org/10.1007/bf00775286

Cinco L., H., Samaniego V., F., & Dominguez A., N. (1978). Transient pressure behavior for a well with a finite-conductivity vertical fracture. *Society of Petroleum Engineers Journal*, *18*(4), 253–264. https://doi.org/10.2118/6014-pa

Cockin, A. P., Malcolm, L. T., McGuire, P. L., Giordano, R. M., & Sitz, C. D. (2000). Analysis of a single-well chemical tracer test to measure the residual oil saturation to a hydrocarbon miscible gas flood at Prudhoe Bay. *SPE Reservoir Evaluation & Engineering*, *3*(6), 544–551.

https://doi.org/10.2118/68051-pa

Cole, J. W., Milner, D. M., & Spinks, K. D. (2005). Calderas and caldera structures: a review. *Earth-Science Reviews*, *69*(1–2), 1–26. https://doi.org/10.1016/j.earscirev.2004.06.004

Davis, J. A., Kent, D. B., Coston, J. A., Hess, K. M., & Joye, J. L. (2000). Multispecies reactive tracer test in an aquifer with spatially variable chemical conditions. *Water Resources Research*, *36*(1), 119–134. https://doi.org/10.1029/1999wr900282

Davis, S. N., Thompson, G. M., Bentley, H. W., & Stiles, G. (1980). Ground-water tracers—a short review. *Ground Water*, *18*(1), 14–23. https://doi.org/10.1111/j.1745-6584.1980.tb03366.x

DiPippo, R. (2016). *Geothermal power plants: Principles, applications, case studies and environmental impact* (4th ed.). Waltham, MA: Butterworth-Heinemann.

Egert, R., Korzani, M. G., Held, S., & Kohl, T. (2020). Implications on large-scale flow of the fractured EGS reservoir Soultz inferred from hydraulic data and tracer experiments. *Geothermics*, *84*, Article 101749. https://doi.org/10.1016/j.geothermics.2019.101749

Erdogmus, B., Toksoy, M., Ozerdem, B., & Aksoy, N. (2006). Economic assessment of geothermal district heating systems: A case study of Balcova-Narlidere, Turkey. *Energy and Buildings*, *38*(9), 1053–1059. https://doi.org/10.1016/j.enbuild.2006.01.001

Faulkner, D. R., Jackson, C. A. L., & Lunn, R. J. (2010). A review of recent developments concerning the structure, mechanics and fluid flow properties of fault zones. *Journal of Structural Geology, 32*(11), 1557–1575. https://doi.org/10.1016/j.jsg.2010.06.009

Fukuda, D., Asanuma, M, Hishi, Y., & Kotanaka, K. (2005). *Alcohol tracer testing at the Matsukawa vapor-dominated geothermal field, northeast Japan*. Paper presented at Thirtieth Workshop on Geothermal Reservoir Engineering, Stanford, CA.

Goko, K. (2000). Structure and hydrology of the Ogiri field, West Kirishima geothermal area, Kyushu, Japan. *Geothermics*, *29*(2), 127–149. https://doi.org/10.1016/s0375-6505(99)00055-3

Grant, M. A., & Bixley, P. F. (2011). *Geothermal reservoir engineering* (2nd ed.). Burlington, MA: Academic Press.

Gringarten, A. C., Ramey, H. J., & Raghavan, R. (1974). Unsteady-state pressure distributions created by a well with a single infinite conductivity vertical fracture. *Society of Petroleum Engineers*

Journal, *14*(4), 347–360. https://doi.org/10.2118/4051-pa

Grove, D. B., & Beetem, W. A. (1971). Porosity and dispersion constant calculations for a fractured carbonate aquifer using two well tracer method. *Water Resources Research*, *7*(1), 128–134. https://doi.org/10.1029/WR007i001p00128

Güven, O., Falta, R. W., Molz, F. J., & Melville, J. G. (1986). A simplified analysis of two-well tracer tests in stratified aquifers. *Ground Water*, *24*(1), 63–71. https://doi.org/10.1111/j.1745-6584.1986.tb01460.x

Hall, S. H. (1993). Single well tracer tests in aquifer characterization. *Ground Water Monitoring and Remediation*, *13*(2), 118–124. https://doi.org/10.1111/j.1745-6592.1993.tb00443.x

Hantush, M. S. (1956). Analysis of data from pumping tests in leaky aquifers. *Transactions, American Geophysical Union*, *37*(6), 702–714. https://doi.org/10.1029/TR037i006p00702

Horne, R. N. (1995). *Modern well test analysis: A computer-aided approach*. Palo Alto, CA: Petroway, Inc.

Houzé, O., Viturat, D., & Fjaere, O. (2012). *Dynamic data analysis: The theory and practice of pressure transient, production analysis, well performance analysis, production logging and the use of permanent downhole gauge data*. Paris: KAPPA Engineering.

International Association for the Properties of Water and Steam (IAPWS) (1997). *Revised release on the IAPS formulation 1985 for the viscosity of ordinary water substance*. Erlangen: International Association for the Properties of Water and Steam.

International Association for the Properties of Water and Steam (IAPWS) (2007). *Revised release on the IAPWS industrial formulation 1997 for the thermodynamic properties of water and steam*. Lucerne: International Association for the Properties of Water and Steam.

Klepikova, M. V., Le Borgne, T., Bour, O., Dentz, M., Hochreutener, R., & Lavenant, N. (2016). Heat as a tracer for understanding transport processes in fractured media: Theory and field assessment from multiscale thermal push-pull tracer tests. *Water Resources Research*, *52*(7), 5442–5457. https://doi.org/10.1002/2016wr018789

Kumagai, N., & Kitao, K. (2000). *Reinjection problems encountered in Sumikawa geothemal power pnant, Japan*. Paper presented at World Geothermal Congress 2000, Kyushu–Tohoku, Japan.

777 Landau, L. D., & Lifshitz, E. M. (1987). Fluid mechanics (2nd ed.) (J. B. Sykes & W. H. Reid, Trans.).
778 *Course of Theoretical Physics* (Vol. 6) (2nd English ed., revised). Oxford: Pergamon Press.

779 Leaf, A. T., Hart, D. J., & Bahr, J. M. (2012). Active thermal tracer tests for improved
780 hydrostratigraphic characterization. *Ground Water*, *50*(5), 726–735.
781 https://doi.org/10.1111/j.1745-6584.2012.00913.x

782 Lemke, D., Liao, Z. J., Wohling, T., Osenbruck, K., & Cirpka, O. A. (2013). Concurrent conservative
783 and reactive tracer tests in a stream undergoing hyporheic exchange. *Water Resources Research*,
784 *49*(5), 3024–3037. https://doi.org/10.1002/wrcr.20277

785 Lemmon, E. W., Jacobsen, R. T., Penoncello, S. G., & Friend, D. G. (2000). Thermodynamic properties
786 of air and mixtures of nitrogen, argon, and oxygen from 60 to 2000 K at pressures to 2000 MPa.
787 *Journal of Physical and Chemical Reference Data*, *29*(3), 331–385.
788 https://doi.org/10.1063/1.1285884

789 Mackay, D. M., Freyberg, D. L., & Roberts, P. V. (1986). A natural gradient experiment on solute
790 transport in a sand aquifer. 1. Approach and overview of plume movement. *Water Resources*
791 *Research*, *22*(13), 2017–2029. https://doi.org/10.1029/WR022i013p02017

792 Matsumoto, M. (2020). A single-phase reservoir simulation method based on a roughly distributed and
793 highly permeable fracture network model with applications to production and reinjection
794 problems. *Geothermics*, *84*, Article 101744. https://doi.org/10.1016/j.geothermics.2019.101744

795 Matsumoto, M. (2022). Data regarding 'Heterogeneity of Subsurface Pore Distribution: Characterization
796 based on Pressure and Tracer Responses to Identify Undiscovered Permeable Structures in
797 Reservoirs' [Dataset]. HydroShare.
798 http://www.hydroshare.org/resource/3b66eb5ff9be4dc19d5e726bf4e08cc7

799 Mroczek, E. K., Milicich, S. D., Bixley, P. F., Sepulveda, F., Bertrand, E. A., Soengkono, S., & Rae, A.
800 J. (2016). Ohaaki geothermal system: Refinement of a conceptual reservoir model. *Geothermics*,
801 *59*, 311–324. https://doi.org/10.1016/j.geothermics.2015.09.002

802 Nakao, S., Ishido, T., & Takahashi, Y. (2007). *Numerical simulation of tracer testing data at the*
803 *Uenotai geothermal field, Japan*. Paper presented at Thirty-Second Workshop on Geothermal
804 Reservoir Engineering, Stanford, CA.

805 O'Sullivan, M. J., Croucher, A. E., Anderson, E. B., Kikuchi, T., & Nakagome, O. (2005). An automated

well-test analysis system (AWTAS). *Geothermics*, *34*(1), 3–25. https://doi.org/10.1016/j.geothermics.2004.08.001

Patidar, A. K., Joshi, D., Dristant, U., & Choudhury, T. (2022). A review of tracer testing techniques in porous media specially attributed to the oil and gas industry. *Journal of Petroleum Exploration and Production Technology*, *12*, 3339–3356. https://doi.org/10.1007/s13202-022-01526-w

Ponte, C., Cabecas, R., Martins, R., Rangel, G., Pham, M., & Klein, C. (2009). Numerical modeling for resource management at Ribeira Grande, Sao Miguel, Azores, Portugal. *Geothermal Resources Council Transactions*, *33*, 847–854.

Pruess, K., & Narasimhan, T. N. (1982). On fluid reserves and the production of superheated steam from fractured, vapor-dominated geothermal reservoirs. *Journal of Geophysical Research*, *87*(NB11), 9329–9339. https://doi.org/10.1029/JB087iB11p09329

Pruess, K., & Narasimhan, T. N. (1985). A practical method for modeling fluid and heat flow in fractured porous media. *Society of Petroleum Engineers Journal*, *25*(1), 14–26. https://doi.org/10.2118/10509-pa

Ptak, T., Piepenbrink, M., & Martac, E. (2004). Tracer tests for the investigation of heterogeneous porous media and stochastic modelling of flow and transport—a review of some recent developments. *Journal of Hydrology*, *294*(1–3), 122–163. https://doi.org/10.1016/j.jhydrol.2004.01.020

Pyrak-Nolte, L. J., Cook, N. G. W., & Nolte, D. D. (1988). Fluid percolation through single fractures. *Geophysical Research Letters*, *15*(11), 1247–1250. https://doi.org/10.1029/GL015i011p01247

Rae, A. J., Cooke, D. R., Phillips, D., & Zaide-Delfin, M. (2004). The nature of magmatism at Palinpinon geothermal field, Negros Island, Philippines: implications for geothermal activity and regional tectonics. *Journal of Volcanology and Geothermal Research*, *129*(4), 321–342. https://doi.org/10.1016/s0377-0273(03)00280-4

Reimus, P., Pohll, G., Mihevc, T., Chapman, J., Haga, M., Lyles, B., et al. (2003). Testing and parameterizing a conceptual model for solute transport in a fractured granite using multiple tracers in a forcedgradient test. *Water Resources Research*, *39*(12), Article 1356. https://doi.org/10.1029/2002wr001597

Rose, P. E., Benoit, W. R., & Kilbourn, P. M. (2001). The application of the polyaromatic sulfonates as

tracers in geothermal reservoirs. *Geothermics*, *30*(6), 617–640. https://doi.org/10.1016/s0375-6505(01)00024-4

Sanjuan, B., Pinault, J. L., Rose, P., Gerard, A., Brach, M., Braibant, G., et al. (2006). Tracer testing of the geothermal heat exchanger at Soultz-sous-Forets (France) between 2000 and 2005. *Geothermics*, *35*(5–6), 622–653. https://doi.org/10.1016/j.geothermics.2006.09.007

Sawayama, K., Ishibashi, T., Jiang, F., Tsuji, T., & Fujimitsu, Y. (2021). Relating Hydraulic–Electrical–Elastic Properties of Natural Rock Fractures at Elevated Stress and Associated Transient Changes of Fracture Flow. *Rock Mechanics and Rock Engineering*, *54*(5), 2145–2164. https://doi.org/10.1007/s00603-021-02391-5

Takaki, M., Itoi, R., & Tanaka, T., (2015). *Laboratory experiment of tracer test in the two-dimensional heterogeneous porous medium*. Paper presented at Fortieth Workshop on Geothermal Reservoir Engineering, Stanford, CA.

Theis, C. V. (1935). The relation between the lowering of the piezometric surface and the rate and duration of discharge of a well using ground water storage. *Transactions, American Geophysical Union*, *16*(2), 519–524. https://doi.org/10.1029/TR016i002p00519

Tomich, J. F., Dalton, R. L., Deans, H. A., & Shallenberger, L. K. (1973). Single-well tracer method to measure residual oil saturation. *Journal of Petroleum Technology*, *25*(FEB), 211–218. https://doi.org/10.2118/3792-pa

Van Everdingen, A. F. (1953). The skin effect and its influence on the productive capacity of a well. *Transactions of the American Institute of Mining and Metallurgical Engineers*, *198*, 171–176.

Van Everdingen, A. F., & Hurst, W. (1949). The application of the Laplace transformation to flow problems in reservoirs. *Transactions of the American Institute of Mining and Metallurgical Engineers*, *186*(12), 305–324. https://doi.org/10.2118/949305-g

Viswanathan, H. S., Ajo-Franklin, J., Birkholzer, J. T., Carey, J. W., Guglielmi, Y., Hyman, J. D., et al. (2022). From fluid flow to coupled processes in fractured rock: Recent advances and new frontiers. *Reviews of Geophysics*, *60*(1), Article e2021RG000744. https://doi.org/10.1029/2021rg000744

Warren, J. E., & Root, P. J. (1963). The behavior of naturally fractured reservoirs. *Society of Petroleum Engineers Journal*, *3*(3), 245–255. https://doi.org/10.2118/426-pa

Yabe, T., & Aoki, T. (1991). A universal solver for hyperbolic-equations by cubic-polynomial interpolation. 1. One-dimensional solver. *Computer Physics Communications*, *66*(2–3), 219–232. https://doi.org/10.1016/0010-4655(91)90071-r

Yabe, T., Ishikawa, T., Wang, P. Y., Aoki, T., Kadota, Y., & Ikeda, F. (1991). A universal solver for hyperbolic-equations by cubic-polynomial interpolation. 2. Two- and Three-dimensional solvers. *Computer Physics Communications*, *66*(2–3), 233–242. https://doi.org/10.1016/0010-4655(91)90072-s

Zarrouk, S. J., & McLean, K. (2019). *Geothermal well test analysis: Fundamentals, applications and advanced techniques*. London: Academic Press.

Zuo, L. H., Tan, X. S., Yu, W., & Hu, X. D. (2019). Fracture detection and numerical modeling for fractured reservoirs. *Energies*, *12*(3), Article 386. https://doi.org/10.3390/en12030386